Materials & Design 225 (2023) 111441

Contents lists available at ScienceDirect

Materials & Design

journal homepage: www.elsevier.com/locate/matdes

Flexible and ultrathin waterproof conductive cellular membranes based on conformally gold-coated PVDF nanofibers and their potential as gas diffusion electrode

Ranxue Yu [a,b,c], Alessandro Senocrate [d,*], Francesco Bernasconi [d,e], Tina Künniger [f], Luca Müller [f], Robin Pauer [g], Corsin Battaglia [d], Xinhou Wang [a,h,*], Jing Wang [b,c,*]

[a] Key Laboratory of Textile Science and Technology of Ministry of Education, College of Textiles, Donghua University, Shanghai 201620, China
[b] Institute of Environmental Engineering, ETH Zurich, 8093 Zurich, Switzerland
[c] Advanced Analytical Technologies, Empa, Ueberlandstrasse 129, 8600 Dübendorf, Switzerland
[d] Empa, Ueberlandstrasse 129, 8600 Dübendorf, Switzerland
[e] Laboratory for Multifunctional Materials, Department of Materials, ETH Zürich, Vladimir-Prelog-Weg 5, 8093 Zürich, Switzerland
[f] Laboratory for Cellulose & Wood Materials, Empa, Ueberlandstrasse 129, 8600 Dübendorf, Switzerland
[g] Electron Microscopy Center, Empa, Ueberlandstrasse 129, 8600 Dubendorf, Switzerland
[h] College of Mechanical Engineering, Donghua University, Shanghai 201620, China

HIGHLIGHTS

- Three-dimensional and conformal gold-coated PVDF nanofibers are successfully fabricated by electrospinning and electroless plating.
- Excellent conductivity, hydrophobicity, and good mechanical flexibility are obtained by microstructural control and gold coating.
- Gold-coated PVDF membranes demonstrate the suitability for electrochemical CO_2 reduction and achieve high current density of 100 mA/cm^2.

GRAPHICAL ABSTRACT

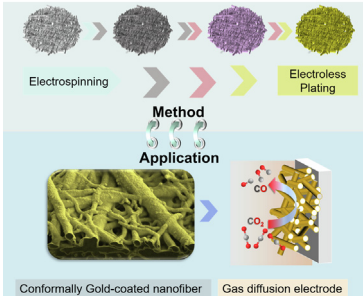

ARTICLE INFO

Article history:
Received 10 July 2022
Revised 29 November 2022
Accepted 29 November 2022
Available online 30 November 2022

Keywords:
Electroless plating

ABSTRACT

Nanofiber membranes (NFMs) coated with noble metals are intensively researched for various applications such as wearable electronics, environmental sensors, and point of care diagnostics. To achieve the desired functionality while minimizing costs, a combination of facile coating methods and accurate microstructural designs is required, but remains elusive. Herein, novel conductive and porous membranes are designed based on a facile and scalable approach to fabricating conformally coated gold layers on electrospun PVDF fibers (Au-PVDF-NFMs) via electroless plating. The deposition of a conformal and fully interconnected gold layer with an average thickness of circa 38 nm on the surface of nanofibers is confirmed by systematic characterizations. The high-conjunction gold layers endows a high electrical

* Corresponding authors at: Empa, Swiss Federal Laboratories for Materials Science and Technology, Dübendorf, Switzerland (A. Senocrate). Donghua University, 2999 North Renmin Road, Songjiang District, Shanghai 201620, China (X. Wang). Institute of Environmental Engineering, ETH Zurich, Zurich, Switzerland, and Empa, Swiss Federal Laboratories for Materials Science and Technology, Dübendorf, Switzerland (J. Wang).

E-mail addresses: Alessandro.Senocrate@empa.ch (A. Senocrate), xhwang@dhu.edu.cn (X. Wang), jing.wang@ifu.baug.ethz.ch (J. Wang).

https://doi.org/10.1016/j.matdes.2022.111441

Conformal and fully interconnected gold layer
Nanofiber
electrochemical CO_2 reduction

conductivity to the membranes, yielding a low sheet resistance of 1.2 Ω/sq. In addition, the membranes show integrated functionalities such as hydrophobicity and gas permeability. Notably, the NFMs also show excellent mechanical durability under both stretching and bending, with negligible conductivity losses after 1000 test cycles. Thanks to these properties, the Au-PVDF-NFMs demonstrates practical suitability as gas diffusion electrodes (GDEs) for electrochemical CO_2 reduction. The Au-PVDF-NFMs exhibit a substantial Faradaic efficiency towards CO, as high as ~ 85 % at −0.7 V vs reversible hydrogen electrode (RHE), and are able to reach current densities of 100 mA cm^{-2} at −0.95 V versus RHE.

1. Introduction

Noble-metal-coated fiber membranes (FMs) with unprecedented conductivity, controllable porosity, and excellent mechanical flexibility are being intensively used due to their potential applications in wearable and flexible electronics,[1,2] energy harvesting,[3,4] sensors for environmental monitoring,[5] and point of care diagnostics.[6] Various inorganic and organic conductive FMs have been exploited, with relevant examples being carbon-based [7,8] and polymer-based substrates.[9,10] Polymer fiber based conductive FMs have the advantages of mechanical flexibility, robustness, tunable pore sizes and can be fabricated through several routes, thus they are widely used for flexible electrodes. [11–13] The polymer used can either be intrinsically conductive, or require the addition of conductive additives or layers.[14] Benefits of the second strategy, which typically uses metals or carbon addition, include higher final membrane conductivity and more flexible and inexpensive processing. To introduce a conductive layer on top of the free-standing polymer FMs substrates (see Table 1), physical vapor deposition,[15–18] chemical vapor deposition,[19,20] and electrochemical plating (EP)[21,22] are commonly used, allowing a rich variety of metal materials to be prepared while retaining excellent electrical conductivity. While precise control over the composition and thickness of these films can be obtained with these methods, they either rely on expensive vacuum equipment or require a conductive polymer substrate for the deposition. Moreover, it remains highly challenging to create three-dimensional conductive networks with controllable structure and morphology with these methods. In contrast, electroless plating (ELP)[23,24] has drawn considerable attention for the preparation of flexible electronic components and 3D conductive networks. ELP is a solution-based, non-electrochemical deposition method relying on a chemical redox reaction to deposit uniform and continuous metallic films on both conductive and non-conductive substrates [25]. It allows for the accurate tuning of the metal thickness and for a conformal surface coverage on rough or nonplanar surfaces, without the directional limitations encountered during physical or chemical vapor deposition.[26] Several works have demonstrated electroless metal plating, e.g. of Ag, Cu, or Pd, on fibrous materials including electrospun carbon nanofibers, PVDF nanofibers, and nonwoven fabrics.[12,24,27,28] Previous reports also showed conformal Au layer deposition, but only on planar substrates [29,30], with no reports discussing deposition on non-planar fiber mats.

In this work, a facile method for producing conformally Au-coated 3D conductive nanofiber membranes (NFMs) is presented, based on electrospun hydrophobic PVDF nanofiber substrates. To the best of our knowledge, this is the first report of conformal Au deposition on nonplanar and hydrophobic PVDF NFMs. The main challenges for the Au deposition arise from the inert and nonplanar surfaces of insulating substrates,[31] from the difficulties to achieve homogeneous distribution on the substrate of the seeds necessary for conformal layer growth[32], as well as from poor Au^{3+} mass transport to the deposition sites.[33,34] To tackle these issues, we first functionalize the substrates with polydopamine (pDA), to enable Au seeds adhesion. Polydopamine (pDA) can absorb on all types of surfaces and give uniformly distributed active sites for metal ion adsorption and metal nucleation.[35,36] We then expose the functionalized surface to Au nanoparticles (NPs), that adhere to the surface and act as seeds for the metal layer growth, allowing a conformal Au layer deposition by ELP.

We systematically characterize both the electrospun NFM substrates and the Au-deposited NFMs by a variety of techniques (scanning and transmission electron microscopy, energy-dispersive X-ray spectroscopy (EDS), X-ray diffraction (XRD), X-ray photoelectron spectroscopy (XPS), porosimetry, pressure drop measurements, dynamic light scattering, and contact angle measurements), to show that we successfully deposit a 38 nm thick, conformal Au layer on the PVDF nanofibers, with no significant alteration to their microstructure. The resulting Au-PVDF-NFMs show a low sheet resistance of 1.2 Ω/sq, alongside an excellent stretching and bending durability giving rise to negligible conductivity loss after 1000 cycles. In addition, the NFMs shows high gas permeability as well as a moderate hydrophobicity. As Au metal is active in the electrochemical CO_2 reduction (CO_2R), we tested the Au-PVDF-NFMs as gas diffusion electrodes for CO_2R. We achieve Faradaic efficiencies towards CO above 75 % at a current density

Table 1
Summary of reported conductive membranes prepared by gold coating on polymers.

Material	Dimensionality	Template	Coating method	Coating thickness	Resistance	Bending durability
Au nanothrough [17]	One layer (2D)[a)]	Eletrospun PVA[b)] /PVP[c)] NFMs[d)]	PVD[e)]	80 nm	2 Ω/sq	1000
Au nanomesh [18]	One layer (2D)	Electrospun PVA NFMs	PVD	70–100 nm	5.3 Ω /sq	10,000
Au /PAN [22]	Top layer (2D)	Electrospun PAN[f)] NFMs	EP[g)] (Pt-Pd seeds)	< 1 μm	N.A.	N.A.
Au/Kapton or PE [29]	Top layer (2D)	Film	ELP[h)] (Plasma + silane)	N.A.	1 Ω/sq	N.A.
Au/PS [30]	Top layer (3D)[i)]	Film	ELP (Plasma + silane + shrinking)	15–55 nm	0.39–1.8 Ω/sq	N.A.
Au/PVDF (this work)	Multilayer (3D)	Electrospun PVDF NFMs[j)]	ELP (pDA)[k)]	38 nm	1.2 Ω/sq	1000

Explanation for abbreviation: [a)] two-dimensional; [b)] polyvinyl alcohol; [c)] polyvinylpyrrolidone; [d)] nanofiber membranes; [e)] physical vapor deposition; [f)] polyacrylonitrile; [g)] electroplating; [h)] electroless plating; [i)] three-dimension; [j)] polyvinylidene fluoride; [k)] polydopamine.

of 100 mA/cm^2, demonstrating the potential use of these membranes in electrocatalysis.

In contrast with previous Au deposition on polymer substrates, Ref [17,18,22,29] in Table 1, which achieved a 2D Au layer deposition of moderate thickness (>70 nm, up to 1000 nm) and conductivity (1–5.3 Ω/sq), this works shows the formation of a 3D Au layer of high conductivity (1.2 Ω/sq), achieved with only a thin coating thickness of 38 nm and thus an efficient use of precious metal. While another work has shown similar performances, (Ref [30] in Table 1) these were achieved with an additional plasma cleaning step, here substituted by the more energetically efficient pDA treatment causing no loss of functional membrane properties.

2. Experimental section

2.1. Chemicals and materials

Polyvinylidene fluoride (PVDF, average Mw = 150000), N, *N*-dimethylformamide (DMF, ACS reagent, ≥ 99.8 %), dopamine hydrochloride (DA-HCl, 98 %), gold (III) chloride solution ($HAuCl_4$, 99.99 % trace metals basis, 30 wt% in dilute HCl), hydrogen peroxide (H_2O_2, 30 wt%), sodium citrate, Tris(hydroxymethyl) aminomethane (99.8 %) were purchased from Sigma-Aldrich. Deionized water from a Milli-Q purification system was used for preparing all the solutions. All the chemicals and materials were used without further purification.

2.2. Electrospinning of nanofiber membranes and hot pressing

PVDF powder was dissolved in a mixture solvent of DMF and acetone in a ratio of 1:1 for 12 h to obtain a 14 % wt PVDF solution. PVDF nanofiber membranes (PVDF-NFMs) were prepared by a multi-jet electrospinning system (NaBond Technologies Co., ltd.) using 20 kV accelerating voltage, 10 cm needle-collector distance and 1 ml·h^{-1} polymer solution flow rate for 2 h. After electrospinning, the membranes were dried in the oven at 60 °C overnight. Prior to surface modification, PVDF-NFMs were compressed via hot-pressing treatment at 125 °C and formed fused junctions. This step eliminated fluffiness and created strong-conjunction points between fiber networks across the NFM thickness, which was beneficial for better mechanical properties of the PVDF-NFMs.[37].

2.3. Electroless Au plating on PVDF-NFMs

2.3.1. Surface modification of PVDF-NFMs

Firstly, 10 mM Tris-HCl buffer solution was prepared by dissolving 0.1211 g Tris (hydroxymethyl) aminomethane (99.8 %) powder in water then 1 M HCl was used to adjust pH at 8.5, followed by addition of water to bring the volume of solution to 100 ml. A 2 g·L^{-1} DA-HCl solution was prepared by dissolving DA-HCl powder in the above 10 mM Tris-HCl solution by sonication. Subsequently, PVDF-NFMs were vertically immersed for 12 h in the freshly prepared DA-HCl solution under stirring. A homogeneous polydopamine (pDA) layer grew on PVDF-NFMs through DA polymerization process. Finally, the PVDF-NFMs with the pDA layer (pDA-PVDF) were ultrasonically cleaned for 2 min to remove overgrown pDA aggregates and washed with deionized water for three times.

2.3.2. Preparation of colloidal AuNPs

All glassware used in the following procedures were cleaned in diluted alkaline solution (Extran MA 01), followed by rinsing thoroughly with deionized water prior to use. Fresh AuNPs seeds were synthesized via reduction of $HAuCl_4$ using citrate sodium as both reducing and stabilizing agent, according to the modified Turkevich method.[38] Briefly, the experiment was performed by adding a $HAuCl_4$ aqueous solution (2.5 ml, 25.4 mM) to 247.5 ml of a boiling citrate aqueous solution (5.2 mM) under vigorous stirring. The solution color turned from light yellow to grey and finally changed to red-wine. After 5 min of boiling, the heating unit was removed and the freshly prepared colloidal AuNPs solution was stored at refrigerator for further use.

2.3.3. Immobilization of AuNPs and ELP of AuNPs onto the pDA-modified PVDF-NFMs

The pDA-modified PVDF-NFMs were vertically immersed in the freshly prepared colloidal AuNPs solution at room temperature for 4 h under stirring. AuNPs were immobilized on the surface of nanofibers by chemical absorption of amino group in PDA to colloidal gold. As a result, those immobilized AuNPs formed a self-assembled monolayer on the PVDF fibers (PVDF-AuNPs), which can be regarded as favorable sites for the seed growth. Subsequently, the PVDF-NFMs was rinsed with deionized water. For ELP, a green reductant and benign reaction condition was employed. The PVDF-AuNPs was immersed in a plating solution containing $HAuCl_4$ and 30 % H_2O_2 for 1 h under stirring at room temperature, where the Au^{3+} reduction reaction occurred at the surface of seed particles.

The key requirement of the ELP method to achieve conformal coating is that the kinetics of homogeneous electron transfer from the reducing agent to the metal ion is slow.[39] Since the reduction $HAuCl_4$ with H_2O_2 is very fast, higher concentrations of $HAuCl_4$ with H_2O_2 will generate higher reduction rates and larger size of AuNPs, which may enhance roughness of NFMs.[40] Herein, we use low concentrations of 0.44 mM $HAuCl_4$ and 15.2 mM H_2O_2 to lower the reaction rate and thus yield uniform AuNPs layer on the surface of nanofibers (defined as Au-PVDF-NFMs). Additionally, mechanical stirring during the ELP process can enable the uniform concentration of $HAuCl_4$ with H_2O_2 around the NFMs, improving the continuity and uniformity of gold nanoparticles on the NFMs surface.

2.4. Materials characterization

Microstructural Analysis: The nanostructure of the colloidal AuNPs used as seeds was analyzed by transmission electron microscopy (TEM) with accelerating voltage 200 kV (JEOL JEM2200FS). Prior to TEM analysis, 5 μl drop of colloidal solution was put on a carbon film copper TEM grid. The TEM grid with the AuNPs droplet was dried in the oven at 60 °C for 1 min. The surface morphology of PVDF-NFMs at different stages of Au deposition and corresponding element mapping were characterized by field emission scanning electron microscopy (FE-SEM, Nova NanoSEM 230, FEI company, Hillsboro, OR, USA). The accelerating voltage is 10 kV and the work distance is circa 5 mm. Generally, 10 nm thickness of Pt (measured with a flat piezo detector) was coated on PVDF-NFMs, pDA-PVDF-NFMs, PVDF-AuNPs to avoid charging. Since the NFMs was too thin to keep the cross section from deformation using the normal cutting process, a combined focus ion beam scanning electron microscope (FIB-SEM, Helios 5UX) was used to evaluate the NFMs' thickness. The cross section was exposed by a FIB milling and imaged by SEM secondary electron mode with the accelerating voltage of 5 kV. Element mapping was done using the EDS system attached to the FIB-SEM system. The atomic force microscopy (AFM (5500 AFM-SPM, Keysight, USA) was used to analyze the surface roughness of NFMs. The obtained images covered an area of 15 μm × 15 μm.

Size Analysis: The size distribution of colloidal AuNPs was further analyzed by dynamic light scattering (DLS) using a Zetasizer Nano Series (Malvern, UK) instrument. The mean diameter of the

fibers comprising the NFMs was determined from FE-SEM images using Image J software, applying a Gaussian fitting.

X-ray Diffraction Analysis: The crystalline structures of Au-PVDF-NFMs were obtained with XRD on a PANalytical X'Pert PRO diffractometer (PANalytical, Netherlands) equipped with Cu Kα radiation. Prior to XRD analysis, the NFMs were taped on the monocrystalline silicone. The operating voltage was 45 kV. The step size was set to 0.083, and the scan range was from 10 to 100°.

XPS Analysis: XPS measurements were carried out on a PHI Quantes spectrometer (ULVAC-PHI) using monochromatic Al Kα radiation (photon energy 1486.6 eV). XPS survey spectra were recorded with a step size of 0.25 eV. The CasaXPS software was used to analyze the XPS data, using the C 1 s signal at 284.8 eV as the reference. Chemical state analysis of element was performed by constrained peak fitting of the Shirley background and setting the ratio of peak area f7: f5 was 4/3 in the same chemical state.

Hydrophobicity Analysis: The static sessile drop method was used to determine the contact angle of water (LiChrosov) on PVDF-NFMs and Au-PVDF-NFMs with a Dataphysics OCA-20 (Germany). The measurements were performed at 20 °C temperature by dropping 1 μl of water on the surface of membranes at three different spots for each sample, taking video images during 30 s, and processed them by an image analysis system.

The sheet resistances of different membranes were measured by a four-probe sheet resistivity meter measurement system (SD-600, NAGY Messsysteme GmbH, Germany). The pore sizes and distribution of membranes were measured by porosimetry (Porolux 1000, Porometer). The NFMs were cut into a 13 mm circle and were impregnated with a wetting liquid. Next, the sample was secured where nitrogen gas was used to displace the liquid out of the porous fiber network. This 'wet run' resulted in a 'wet curve' which represented the measured gas flow through the sample against the applied pressure. The same method as above was used for a dry sample ('dry run') measurement. According to wet and dry curve, we obtained the pore size and distributions of NFMs.

Mechanical Analysis: The tensile test was conducted by tensile tester (Zwick, Z010). The initial loading is 0.05 N and loading speed is 2 mm/min. The NFMs' size was in 20 mm × 4 mm (length × width). The mechanical stability of the samples, including bending and stretching was evaluated by a home-built bending test instrument and by a dynamic mechanical analyzer (DMA, TA Q800). The pressure drops when CO_2 passing through PVDF-NFMs and Au-PVDF-NFMs were measured by a pressure transducer (PC409, Omega, Inc.). The projected area for measurement was 9.62 cm^2. The CO_2 flow rate was tuned by a mass flow controller (Aalborg TIO totalizer). The intrinsic gas permeability (k) of a material can be calculated according to Darcy' law as the following equation (1) [41]:

$$k = \frac{Q\mu L}{A\Delta P} \tag{1}$$

where Q is the fluid flux, A is the cross-section area, μ is the fluid viscosity, which is 1.48 × 10^{-5} Pa s for CO_2[42], L is the thickness of the media, Δ P is the pressure drop across the media.

2.5. CO_2 electrochemical measurements and product analysis

The electrochemical CO_2R was tested in a two-compartment cell (an image of flow cell configuration can be found in SI Fig. S1). The working electrode, that is the cathode for the CO_2R, was the Au-PVDF-NFMs. The reference electrode was an Ag/AgCl electrode, and an oversized Ti gauze coated with IrO_x was used as the counter electrode. 0.1 M $KHCO_3$ solution was used as the electrolyte. We chose this electrolyte as it has been demonstrated previously that the selectivity toward CO was optimal in this concentration of electrolytes, and to reduce water permeation through the anion exchange membrane induced by high cation concentrations.[43–45] For the electrochemical measurement, Au-PVDF-NFMs were hot pressed on an anion exchange membrane (AEM, Sustainion™, PTFE supported) to obtain a membrane-electrode assembly (MEA). Subsequently, the MEA was encapsulated in Teflon tape with an exposed geometric electrode area of 0.196 cm^2. The MEA was fixed between the two electrolysis cell compartments, and the electrolyte was added to the chamber facing the AEM. The counter electrode was immersed in the electrolyte. The Au-PVDF-NFMs was in contact with gaseous CO_2 while the AEM contacted the electrolyte. During the electrolysis experiments, CO_2 was introduced with a flow rate of 30 ml min^{-1} for sufficient CO_2 transport to the electrode surface. CO_2 was purged into the reaction system for 30 min to reach pH equilibrium. The flow rate was regulated by a mass flow controller (FL-201CV, Bronkhorst, HIGH-TECH, Germany). All the electrode potentials were converted to RHE scale. All the electrochemical experiments were conducted at room temperature. A Biologic SP240 potentiostat was used for CO_2R electrochemical measurements. In a typical experiment, a linear scan voltammetry was initially used to bring the sample to the appropriate reduction voltage. Subsequently, a chronoamperometric step was performed at the desired reduction voltage for 1 h, while simultaneously analyzing the reaction products leaving the electrolyzer cell by gas chromatography. The current densities obtained were normalized to the geometric surface area.

The *FE* of gas products was evaluated according to equation (2):

$$FE_i = \frac{e_i \times F \times P \times V \times X_i}{J \times R \times T} \times 100 \tag{2}$$

where e_i is the number of transferred electron (herein is 2 for H_2 and CO), F is the Faradaic constant (96485.3 A·s·mol^{-1}), P is atmospheric pressure (101.3 kPa), V is the volumetric flow rate of CO_2, X_i is the concentration of the product measured by gas chromatography, J is the total current measured by the potentiostat.

3. Results and discussion

3.1. Preparation of electrospun Au-PVDF-NFMs

As presented in Fig. 1, we prepare the Au-PVDF-NFMs starting from electrospinning the PVDF substrate and hot pressing (Step 1 and 2), and subsequently depositing Au via a three-step process including activation of the PVDF surface (Step 3), immobilization of Au seeds (Step 4), and ELP (Step 5). We fabricate electrospun fiber mats starting from a concentrated solution of PVDF in DMF/acetone. After drying and hot pressing, the polymer nanofibers are crosslinked together and the NFMs become compact. These compact polymer fibers and fused conjunctions are critical for the subsequent electroless gold plating, significantly reducing the contact resistance and improving conductivity after metal deposition. The thickness of the membranes can be adjusted by varying the spinning time. A membrane with a thickness around 15 μm can be obtained after a continuous 2 h electrospinning. The control of membrane thickness allows to tune the porosity of gas diffusion electrodes, further regulating the diffusion mass transport of reactant to electrode. A relatively thin membrane will greatly reduce the diffusion path and enable high-rate gas transport.

We subsequently activate the surface of the PVDF-NFMs by a self-assembled pDA layer via a dopamine self-polymerization process under basic conditions. Previous literature reveals that terminal functional groups on the polymer such as thiol (–SH), amino (–NH_2) and cyanide (–CN) have high affinity to colloidal gold.[35,46] The deposited pDA has terminal amino groups, which upon exposure to colloidal AuNPs are able to bind the gold nanoparticles on

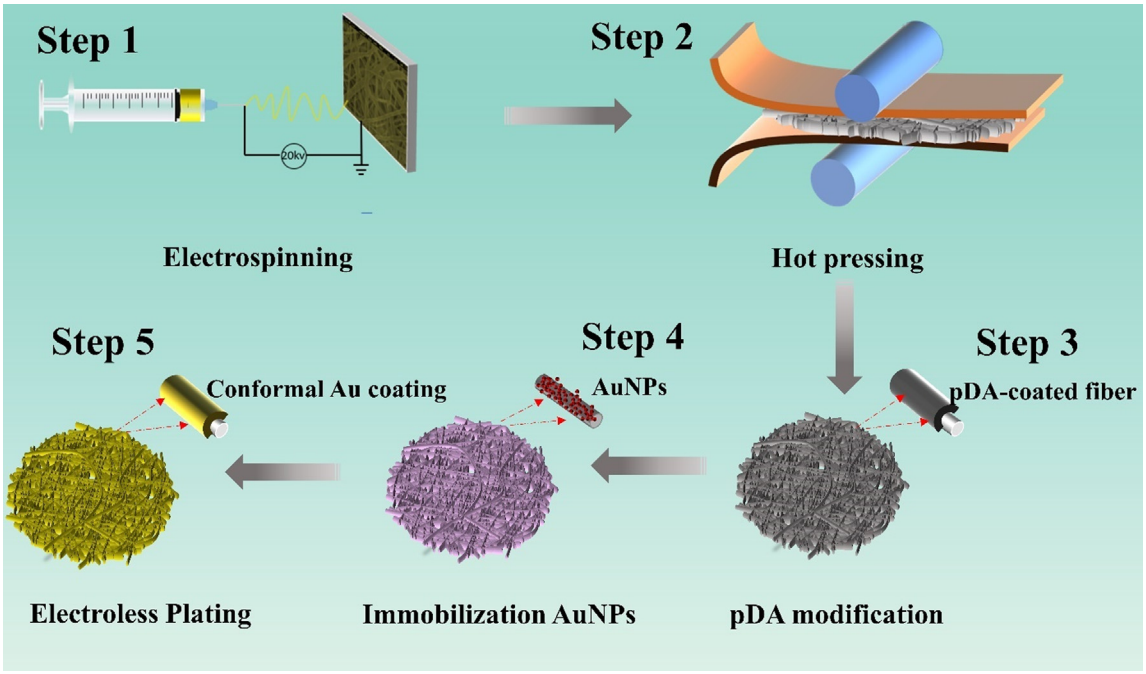

Fig. 1. Schematics of the fabrication of Au-coated electrospun PVDF nanofiber membranes.

the surface of the nanofibers. In order to obtain highly conductive Au electrodes, we subsequently conduct ELP using H_2O_2 as green reductant for Au^{3+} ions. As expected, the AuNP act as seeds for the Au layer growth by providing favorable nucleation center for the Au^{3+} reduction. Thus, a conformal layer is formed on the NFM without any Au nucleation in solution.[40] We expect that during ELP, O_2 bubble formation ($2\,AuCl_4^- + 3\,H_2O_2 \rightarrow 2\,Au + 8Cl^{-1} + 3\,O_2$, E= + 0.307 V) from the parasitic H_2O_2 reduction will also take place on the NFM surface and thus induce porosity in the Au layer.[47] We therefore apply vigorous stirring during this step to remove the O_2 bubbles, obtaining a homogeneous and compact Au layer. Besides, the above compact PVDF-NFMs via hot pressing will suppress the big O_2 bubble formation and improve sufficient mass transport, leading the homogeneity of gold coating.

3.2. Characterization of Au-PVDF-NFMs

Fig. 2 shows the SEM images and fiber diameter distributions of the PVDF-NFMs through several steps of the Au deposition. SEM images of electrospun PVDF NFMs given in SI Fig. S2 reveal the formation of polymer conjunctions after the hot-pressing step, owing to the melting of PVDF nanofibers. These fused regions boost the mechanical strength of membranes and improve the compactness of nanofibers, which is helpful for handling and practical use of the membranes as electrodes. Fig. 2a1-a3 show the electrospun PVDF-NFMs after hot pressing, presenting a highly porous structure with a mean fiber diameter of 358 nm. Fig. 2b1-b3 show that after pDA modification and ultrasonic cleaning, the resulting NFMs possess a smooth and conformal pDA layer, which facilitates the formation of the conformal Au layer. Besides, the conformal and well-ordered pDA layer has high tolerance to mechanical deformation. The mean diameter of pDA-modified electrospun nanofibers remains similar as before the modification. Compared with relevant works utilizing plasma and silane treatment, an eco-friendly and simple pDA treatment is employed here, maintaining the conformal surface of the membrane's substrates. In addition, we find that silane treatment easily results in agglomerates of colloidal AuNPs due to the formation of silane multilayer.[48] Fig. 2c1-c3, show the NFMs after exposure to the AuNPs solution, which leads to NPs grafting and to the formation of a well-ordered and non-continuous Au seed layer. This PVDF-AuNPs-NFMs is not conductive as verified by a multimeter. The AuNPs used have an average diameter of 13 nm, as shown by the TEM image of Fig. 3a and additional SI Fig. S3. The thin and uniform AuNP layer serves as the nucleation sites for the Au deposition via ELP. During ELP, as shown in Fig. 2d1-d2, the AuNPs first grow into large nanoparticles, then coalesce and finally form a continuous and complete Au layer with residual AuNPs agglomerates on the fiber surface, in agreement with previous literature.[31,40] As shown in Fig. 2a3-d3, we observe no significant difference in the fiber diameter distribution after the various deposition steps.

Using FIB milling, we obtain the cross section shown in Fig. 3b, which highlights the efficient formation of core–shell gold-coated structures in the cellular membranes. Through these images, we estimate that the average Au layer thickness is circa 38 nm. Elemental spectrum and elemental mapping of the surface and cross section of the Au-PVDF-NFMs are given in Fig. 3c, SI Fig. S4 and SI Fig. S5. The mappings show a homogeneous and fully connected Au distribution on the polymer fibers. The root-mean-square surface roughness of gold coating in fiber is about 100 nm, further confirming the conformal gold coating on PVDF nanofibers as shown in the AFM topographic image and a high-resolution AFM image (Fig. 3d and 3e). Despite gold deposition on both sides of the membranes, the resulting Au-PVDF-NFMs retain a good membrane flexibility, as shown in SI Fig. S6. Upon carrying out ELP deposition at room temperature for 1 h, the resulting Au-PVDF-NFMs have a low sheet resistance of 1.2 Ω/sq. The conformal and fully interconnected gold layer on the polymer nanofibers contributes to the high conductivity of Au-PVDF-NFMs, rendering them excellent candidates for flexible gas diffusion electrodes.

The crystalline structure and chemical state of AuNPs play vital role in the potential application of conformally gold-coated PVDF-NFMs. Fig. 4a shows the XRD patterns of PVDF-NFMs at different stages of the Au deposition. No Au diffraction peaks are visible in PVDF-NFMs and after pDA activation, while a diffraction peak at 38.2°, corresponding to the Au (111) plane, appears in the mem-

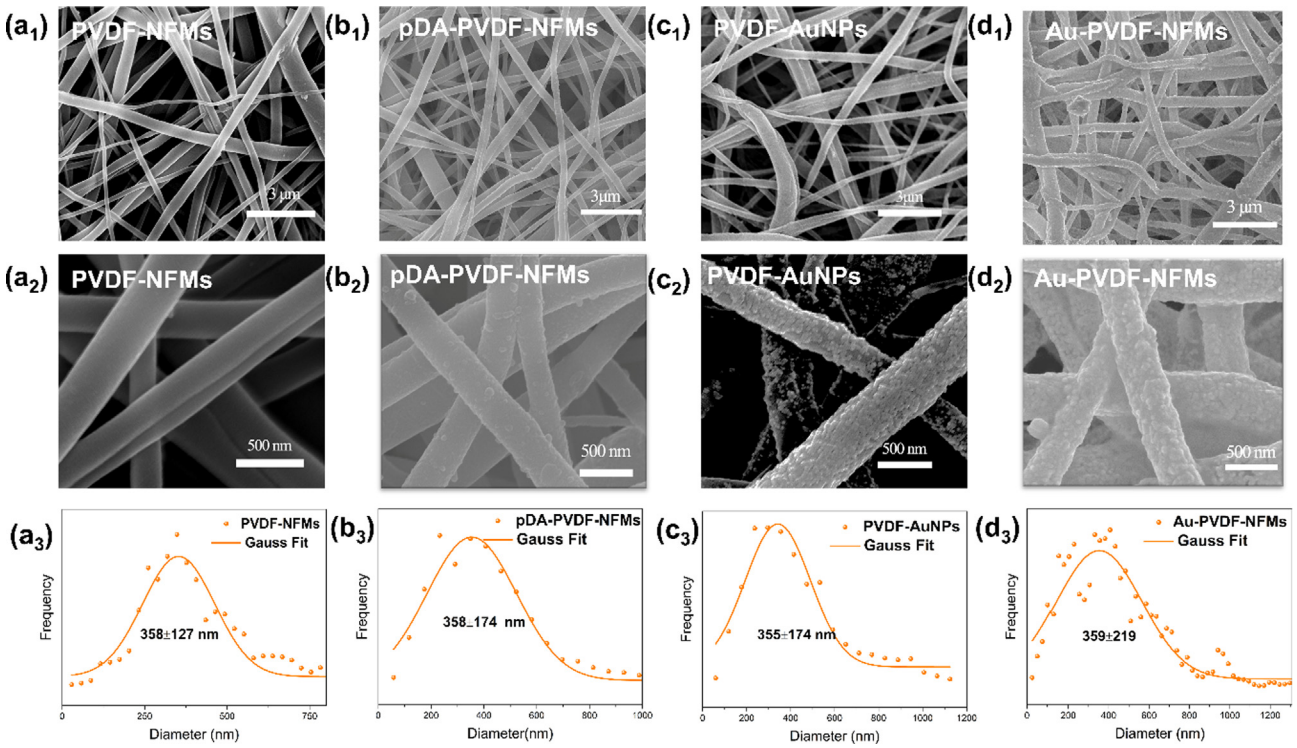

Fig. 2. Electrospun membranes at different stages of the Au deposition. **(a)** Pristine electrospun PVDF, **(b)** After pDA coating, **(c)** After AuNPs immobilization, and **(d)** After Au layer deposition by ELP. **(a1-d1)**, SEM images, **(a2–d2)** High-resolution SEM images, **(a3–d3)** Fiber diameter distributions evaluated from the SEM images with their corresponding Gaussian fittings.

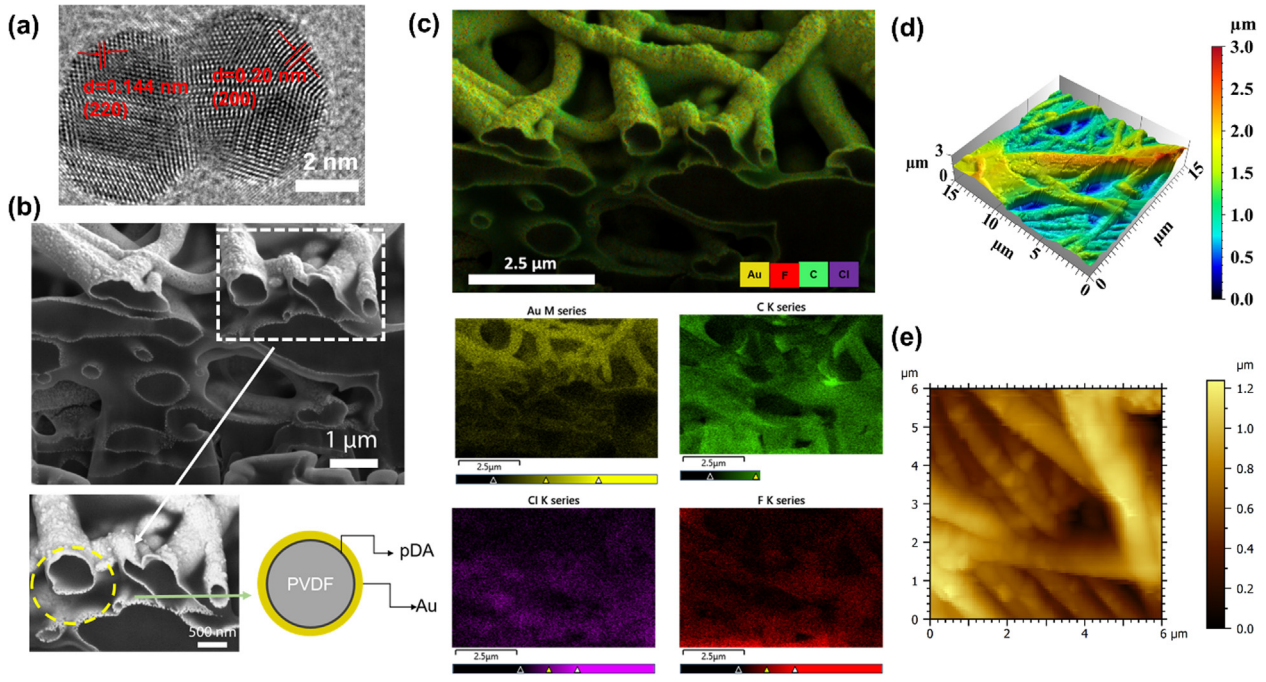

Fig. 3. **(a)** TEM image of AuNPs capped by sodium citrate. **(b)** Cross-sectional SEM image of Au-PVDF-NFMs, high-resolution SEM image from the selected region and scheme of the composition of each layer of an Au-PVDF nanofiber. The cross section was prepared by FIB milling. **(c)** Elemental mapping for Au, C, F and Cl in the same area imaged in panel **(b)**. **(d)** The topographic images of Au-PVDF-NFMs by AFM with the size of 15 μm × 15 μm. **(f)** High-resolution AFM image captured from the selected region in (d).

branes after Au seeding and grows strongly after the ELP step. In this latter diffractogram, four additional weaker peaks are present at 44.5° from Au (200), 64.6° from Au (220), 77.6° from Au (311) and 81.7° from Au (222). These peaks are consistent with the TEM results on AuNPs, given in Fig. 3a, which shows a crystalline unit composed of two Au (200) and (220) planes, confirming the polycrystalline nature of the seeds. Additionally, the much stronger peak at 38.2° indicates a preferential growth of the Au layer along the (111) plane during the ELP process. This result agrees with pre-

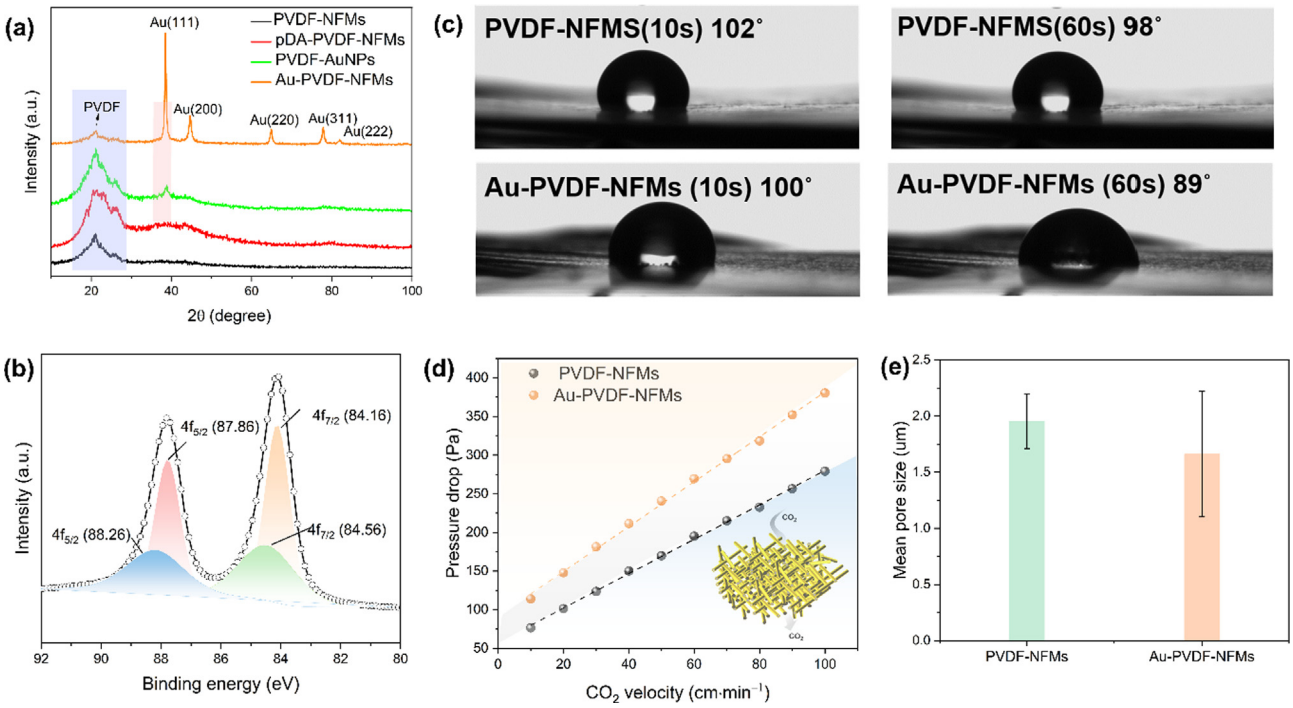

Fig. 4. (**a**) X-ray diffraction patterns of PVDF-NFMs, pDA-PVDF-NFMs, PVDF-AuNPs and Au-PVDF-NFMs. (**b**) XPS spectra of Au-PVDF-NFMs. The black line represents the raw data and the other color lines are the fitting result. (**c**) Photographs of Water drops and water contact angle on the surface of PVDF-NFMs and Au-PVDF-NFMs after 10 and 60 s. (**d**) Measured CO_2 pressure drops through the PVDF-NFMs and Au-PVDF-NFMs as functions of the CO_2 face velocity. (**e**) The mean pore sizes of PVDF-NFMs and Au-PVDF-NFMs measured by gas–liquid porosimetry.

vious literature reports of oriented layer growth during Au deposition by ELP.[31,49].

We also investigate the surface chemistry and oxidation state of the Au-PVDF-NFMs via XPS. As shown in Fig. 4b, and additionally in SI Fig. S7, Au-PVDF-NFMs present two peaks at binding energies of 84.16 eV and 87.86 eV corresponding to $Au4f_{7/2}$ and $Au\ 4f_{5/2}$ bands, confirming the effective deposition of a metallic Au^0 layer. [50] Additional peaks of the spectra with positive shift of 0.4 eV are identified as Au (I), possibly due to the incomplete $AuCl_4^-$ reduction by H_2O_2.

Conductive, flexible, and porous NFMs could find application as sensors, gas diffusion electrodes, or in wearable electronics. For such applications, relevant properties are conductivity, hydrophobicity (if in contact with an aqueous electrolyte), and gas permeability. Thus, we use a hydrophobic PVDF-NFMs substrate for the electrode. We first analyze the hydrophobicity of PVDF-NFMs and Au-PVDF-NFMs by water contact angle (WCA), shown in Fig. 4c. The PVDF-NFMs show a stable WCA of 102° with minor decrease along the time, indicating strong hydrophobicity. However, as expected from the conformal and hydrophilic pDA and Au coatings,[51] the final Au-PVDF-NFMs show a decrease of 2° in WCA compared to PVDF-NFMs, which is also a little unstable with the time. The hydrophobic microenvironment around the interfaces of Au-PVDF-NFMs can efficiently prevent flooding of the pores in the cellular membranes.

We then move on to study the gas permeability and pore size distribution of the Au-PVDF-NFMs. The CO_2 pressure drop measurements through a 15 μm Au-PVDF-NFM were carried out using different CO_2 face velocities in the range of 10 to 100 $cm{\cdot}min^{-1}$. As shown in Fig. 4d, the pressure drop linearly increases with increasing CO_2 face velocity. For the Au-PVDF-NFMs, a pressure drop of 100 Pa (0.001 bar) at the velocity of 30 $ml{\cdot}\ min^{-1}$ using for the electrochemical CO_2 reduction is calculated based on a projected area of 9.62 cm^2 and linear equation (y = 2.90 × + 91.44) across the membrane. Using Darcy's law[52] we obtain an intrinsic permeability of 1.275 × 10^{-14} m^2 for CO_2.This low gas resistance is an advantage for applications such as gas diffusion electrodes. We also investigate possible changes in the pore size distribution of PVDF-NFMs and Au-PVDF-NFMs, i.e., before and after Au deposition, using porosimetry. As shown in Fig. 4e, the mean pore size is 1.9 ± 0.24 μm and 1.7 ± 0.56 μm before and after Au coating, respectively, demonstrating the marginal influence of the Au layer on the pore size. The abundant and interconnected pores in the Au-PVDF-NFMs provide sufficient pathways for gas transport, rendering them excellent candidates as gas diffusion electrode.

Good mechanical properties facilitate scalable preparation of the flexible and conductive membranes. We characterize the mechanical properties of the Au-PVDF-NFMs with the tensile strength testing setup schematized in SI Fig. S8. As shown in Fig. 5a, the Au coating causes an increase in Young's modulus and thus a partial loss of elasticity and reduced fiber elongation compared to uncoated PVDF NFMs. The increased Young's modulus arises from the robust adhesion of the pDA interlayer that strongly links the gold layer and the nanofibers. We also investigate the resilience of the membranes to deformation stress, using the membrane conductivity as an indicator for the stability of the metal layer under stress. Fig. 5b shows that we are able to power an LED lamp by flowing current from a battery through the Au-PVDF-NFM under bending, twisting or stretching stress, indicating stable conductivity under various deformations. To be more quantitative, we perform stretching and bending cycles on the Au-PVDF-NFMs and monitor changes in resistance for signs of layer instability using the DMA unit and home-made bending testing unit, respectively. As seen in Fig. 5c, 1000 stretching cycles at 2 % strain cause a minor 20 % increase in resistance of the Au-PVDF-NFM, measured along the longitudinal direction. The resistance increase only takes place within the first 50 cycles, while the fibers show a stable behavior (<5 % additional loss) afterwards, indicating

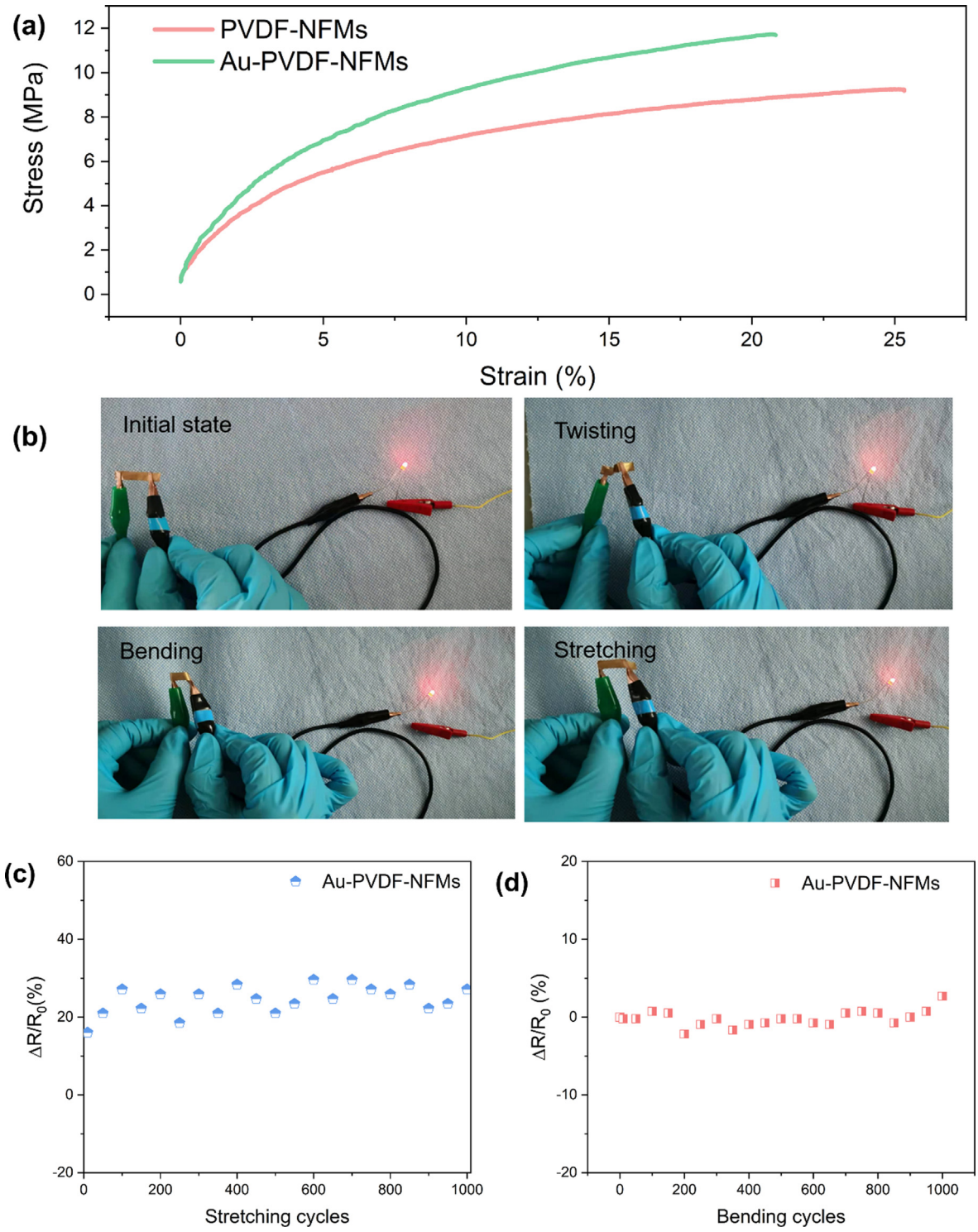

Fig. 5. **(a)** Typical tensile curves of PVDF-NFMs and Au-PVDF-NFMs. **(b)** Photograph of conductive Au-PVDF-NFMs under twisting, bending and stretching. **(c)** Resistance changes versus stretching-recovery cycles, the stretching strain was set as 2%. **(d)** Resistance changes versus bending-recovery cycles.

that the conductivity loss is due to an initial adaptation of the conductive layer to the applied stress. Concerning bending, Fig. 5d shows that the resistance of Au-PVDF-NFMs does not obviously change even after 1000 bending cycles from 0° to 180°. The microstructural characteristics (conformal and interconnected gold-coated fiber networks) and the strong adhesion from pDA layer linking the metal layer and nanofibers endow Au-PVDF-NFMs with a high resistance to various mechanical deformations, leading to the remarkable conductive stability of Au-PVDF-NFMs. Besides, the strong conjunction points formed by hot pressing connecting conductive nanofibers also boost the mechanical strength and conductive stability as seen in Fig. S9.

3.3. Electrochemical properties of Au-PVDF-NFMs

An efficient microstructural design is essential for several potential applications. Au-PVDF-NFMs show excellent conductivity, moderate hydrophobicity, controllable porosity, and excellent mechanical flexibility. Due to their above-mentioned merits, and the known electrocatalytic activity of Au,[53] we apply Au-PVDF-NFMs as gas diffusion electrode for electrochemical CO_2R, specifically as cathodes. For the testing, the Au-PVDF-NFMs are laminated on top of an anion exchange membrane to form a membrane electrode assembly (MEA). A schematic of the fabricated MEAis depicted in Fig. 6a. The 3D fiber networks improve diffusion mass transport of gases to and from the electrode.An oversized IrO_x anode coated on a Ti gauze completes the electrochemical cycle by oxidizing H_2O to O_2. We start by performing cyclic voltammetry (CV) of Au-PVDF-NFM GDEs exposed to Ar-saturated and CO_2-saturated environments. As shown in Fig. 6b, the GDEs show a higher current density in CO_2-saturated electrolytes, confirming that the Au-PVDF-NFMs are active towards CO_2 reduction (Fig. 6b). In the Ar-saturated environment, only the competing hydrogen evolution reaction (HER) takes place. We evaluated the catalytic performance of Au-PVDF-NFM GDEs by constant potential experiments between −0.5 to −1 V vs RHE, coupled with gas analysis of the products. As shown in Fig. 6c, the GDEs yield substantial amounts of CO as a CO_2 reduction product, with a maximum FE_{CO} ~ 85 % at −0.7 V vs RHE. The remaining FE is accounted for by the HER producing H_2 gas. As shown in Fig. 6d, the Au-PVDF-NFM GDEs are able to achieve a high current density of 100 mA cm^{-2} at −0.95 V vs RHE, possibly due to the improved diffusion mass transport and resultant extended active surface area. Lastly, we systematically characterize the variations in surface morphology, hydrophobicity and chemical state of our Au-PVDF-NFMs after the electrode is operated at −0.7 V for 1 h (Fig. 6e, f, h). We find that Au-PVDF-NFMs remain unchanged in physical properties, demonstrating an excellent structural stability. For better performance in the electrochemical reduction of CO_2, a balance between gas and liquid in the GDEs during the electrolysis is also crucial. If the electrode becomes hydrophilic, the pores in the catalyst layer will be blocked by the electrolytes, which will suppress the gaseous CO_2 close to catalyst and lead to a decline of the reaction rate. The differential pressure across the interface between the liquid and gas is determined using the Young-Laplace equation [54]: $P_{liquid} - P_{gas} = 2\sigma \sin(\theta - 90^{\circ})/r$, where σ is the surface tension of 0.1 M $KHCO_3$ electrolytes (assuming the same as water, 72 mN

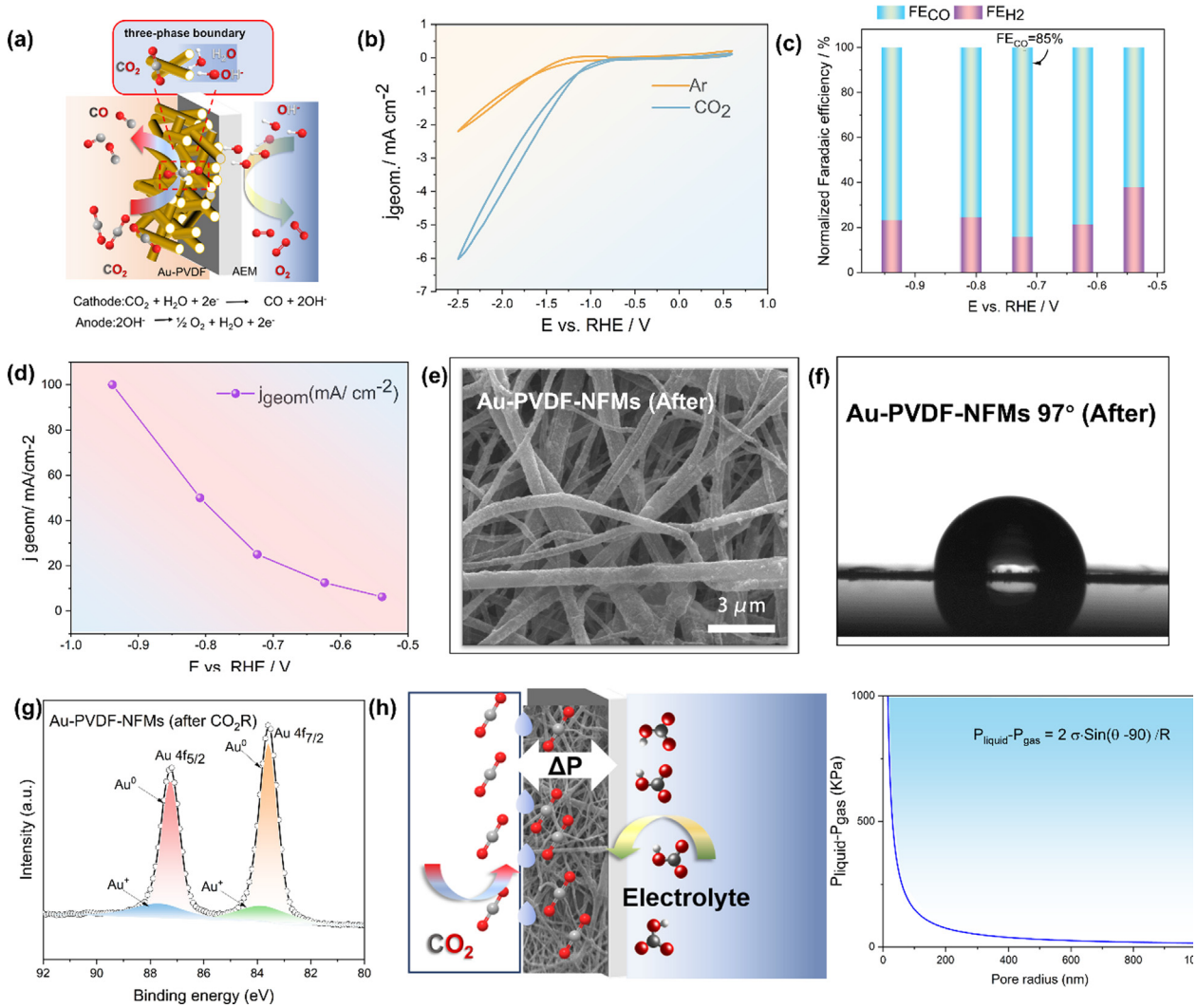

Fig. 6. **(a)** Schematic representation of the Au-PVDF-NFMs as gas diffusion electrode system studied in this work. **(b)** CV of the Au-PVDF-NFMs under CO_2 or Ar gas flow. **(c)** Normalized Faradaic efficiencies for CO and H_2, each point is a 1 h chronoamperometry experiment **(d)** Current densities for CO_2R at −0.5 to −1 V. **(e)** SEM images, (f) Photographs of contact angle measurements and **(g)** XPS spectra of gold on the Au-PVDF-NFMs electrode after CO_2 electrolysis at −0.7 V for 1 h. **(h)** Schematic presentation of the differential pressure across the liquid–gas interface and the differential pressure as a function of the pore radius.

m^{-1}), θ is the contact angle of electrolytes on the Au-PVDF-NFMs and r is the pore radius. Based on above equation, a greater hydrophobicity and a smaller pore will generate a higher pressure for liquid to enter the pore and suppress flooding. As plotted in Fig. 6h, the differential pressure of our Au-PVDF-NFMs with a thickness of 15 μm is so low that easily resulting in the flooding of electrolytes.

These preliminary results indicate a potential application of these conformally coated NFMs as gas diffusion electrodes for electrocatalytic reactions. Nonetheless, the GDEs hydrophobicity is only moderate, leading to flooding and reduced stability during electrochemical experiments, and presenting a clear drawback. Additionally, electro-wetting of the catalyst layer upon application of a negative voltage can further accelerate the flooding.[55] Therefore, further work addressing water management, for example by acting on the pore size of the Au-PVDF-NFMs or by adding polytetrafluoroethylene particles will be essential to create a stable and hydrophobic microenvironment for efficient CO_2 electrolysis.[56].

4. Conclusions

In this work, we develop a facile, flexible, and scalable method for the preparation of novel conductive and cellular membranes by fabricating conformally coated gold layers on the hydrophobic electrospun PVDF fibers via electroless plating. Porous electrospun PVDF NFMs are activated with a pDA layer, deposited with a seeding layer of Au NPs and finally coated by electroless plating with a conformal, uniform Au layer of 38 nm thickness. The success of the 3D conformal deposition, as well as the high quality and stability of the Au layer is confirmed by systematic structural, microstructural, and electrical analyses. In particular, the high-conjunction gold coating yields a low membrane sheet resistance of 1.2 Ω/sq and an excellent mechanical durability under stretching and bending, with negligible resistance increase after 1000 test cycles. In contrast with other methods, the use of electrospinning yields substrates that are potentially scalable and microstructurally controllable, while the metal deposition achieves a three-dimensional, conformal coating on hydrophobic and nonplanar substrates, with no plasma treatment and no metal agglomeration, requiring only environmentally friendly reagents. Additionally, the strong adhesion between pDA and Au layer makes the coating layer more stable resisting deformation. Moreover, comparing with other previous work, the conformal and high-conjunction Au layer in the thinner thickness makes them more conductive.

With the efficient microstructure design, the samples are demonstrated to have practical suitability as GDEs for CO_2R showing a Faradaic efficiency towards CO ~ 85 % at −0.7 V vs RHE, and a high current density of 100 mA/cm^2 at −0.95 V vs RHE. Future directions of interest for this and other applications could consider changes in the AuNPs shape to control the final Au layer crystalline structure, variation in polymer chemistry and substrate microstructure to tune the mechanical properties, hydrophobicity and gas permeability of the membranes, as well as the use of hydrophilic and/or conductive substrates for the electroless deposition.

CRediT authorship contribution statement

Ranxue Yu: Conceptualization, Data curation, Formal analysis, Writing – original draft. **Alessandro Senocrate:** Investigation, Formal analysis, Supervision, Writing – review & editing. **Francesco Bernasconi:** Methodology, Software. **Tina Künniger:** Methodology, Software. **Luca Müller:** Methodology. **Robin Pauer:** Methodology. **Corsin Battaglia:** Methodology. **Xinhou Wang:** Supervision, Funding acquisition. **Jing Wang:** Conceptualization, Supervision, Writing – review & editing.

Data availability

No data was used for the research described in the article.

Declaration of Competing Interest

The authors declare that they have no known competing financial interests or personal relationships that could have appeared to influence the work reported in this paper.

Acknowledgments

Ranxue Yu acknowledges the China Scholarship Council and Donghua University for the financial support. She also thanks the National Natural Science Foundation of China (Grant No. 51776034) for the support. She thanks Beatrice Fischer for her guidance in mechanical test. She also acknowledges the support from the Scientific Center for Optical and Electron Microscopy (ScopeM) of the ETH Zurich, especially from the ScopeM staff Peng Zeng.

Appendix A. Supplementary material

Supplementary data to this article can be found online at https://doi.org/10.1016/j.matdes.2022.111441.

References

[1] J. Lee, H. Kwon, J. Seo, S. Shin, J.H. Koo, C. Pang, S. Son, J.H. Kim, Y.H. Jang, D.E. Kim, T. Lee, Conductive fiber-based ultrasensitive textile pressure sensor for wearable electronics, Adv. Mater. 27 (15) (2015) 2433–2439.
[2] A. Chinnappan, C. Baskar, S. Baskar, G. Ratheesh, S. Ramakrishna, An overview of electrospun nanofibers and their application in energy storage, sensors and wearable/flexible electronics, J. Mater. Chem. C 5 (48) (2017) 12657–12673.
[3] C.-T, Dinh, T, Burdyny, M.G, Kibria, A, Seifitokaldani, C.M, Gabardo, F.P.G.d, Arquer, A, Kiani, J.P, Edwards, P.D, Luna, O.S, Bushuyev, C, Zou, R, Quintero-Bermudez, Y, Pang, D, Sinton, E.H, Sargent, CO electroreduction to ethylene via hydroxide-mediated copper catalysis at an abrupt interface, Science 360(6390) (2018) 783-787.
[4] S. Jayaraman, V. Aravindan, P. Suresh Kumar, W. Chui Ling, S. Ramakrishna, S. Madhavi, Exceptional Performance of TiNb2O7 anode in all one-dimensional architecture by electrospinning, ACS Appl. Mater. Interfaces 6 (11) (2014) 8660–8666.
[5] J. Gao, H. Wang, X. Huang, M. Hu, H. Xue, R.K. Li, A super-hydrophobic and electrically conductive nanofibrous membrane for a chemical vapor sensor, J. Mater. Chem. A 6 (21) (2018) 10036–10047.
[6] G. Chen, X. Xiao, X. Zhao, T. Tat, M. Bick, J. Chen, Electronic textiles for wearable point-of-care systems, Chem. Rev. 122 (3) (2022) 3259–3291.
[7] S. Liu, M. Kok, Y. Kim, J.L. Barton, F.R. Brushett, J. Gostick, Evaluation of electrospun fibrous mats targeted for use as flow battery electrodes, J. Electrochem. Soc. 164 (9) (2017) A2038–A2048.
[8] Y. Xu, Y. Zhang, Z. Guo, J. Ren, Y. Wang, H. Peng, Flexible, stretchable, and rechargeable fiber-shaped zinc-air battery based on cross-stacked carbon nanotube sheets, Angew. Chem., Int. Ed. 54 (51) (2015) 15390–15394.
[9] J. Li, G. Chen, Y. Zhu, Z. Liang, A. Pei, C.-L. Wu, H. Wang, H.R. Lee, K. Liu, S. Chu, Y. Cui, Efficient electrocatalytic CO2 reduction on a three-phase interface, Nat. Catal. 1 (8) (2018) 592–600.
[10] G.O. Larrazábal, P. Strøm-Hansen, J.P. Heli, K. Zeiter, K.T. Therkildsen, I. Chorkendorff, B. Seger, Analysis of mass flows and membrane cross-over in CO2 reduction at high current densities in an MEA-Type Electrolyzer, ACS Appl. Mater. Interfaces 11 (44) (2019) 41281–41288.
[11] Y. Fujiwara, K. Shibasaki, M. Takahashi, S. Ikeda, Y. Kobayashi, Cu-Sn alloy microtube assembly fabricated by electroless plating on polyester nonwoven fabric and its lithiation-delithiation performance, Appl. Surf. Sci. 493 (2019) 112–124.
[12] W. Ju, F. Jiang, H. Ma, Z. Pan, Y.B. Zhao, F. Pagani, D. Rentsch, J. Wang, C. Battaglia, Electrocatalytic reduction of gaseous CO2 to CO on Sn/Cu-nanofiber-based gas diffusion electrodes, Adv. Energy Mater. 9 (32) (2019) 1901514.
[13] B. Bessaire, M. Mathieu, V. Salles, T. Yeghoyan, C. Celle, J.-P. Simonato, A. Brioude, Synthesis of Continuous Conductive PEDOT:PSS nanofibers by electrospinning: a conformal coating for optoelectronics, ACS Appl. Mater. Interfaces 9 (1) (2017) 950–957.

[14] X. Li, X. Chen, Z. Jin, P. Li, D. Xiao, Recent progress in conductive polymers for advanced fiber-shaped electrochemical energy storage devices, Mater. Chem. Front. 5 (3) (2021) 1140–1163.
[15] P.A. Pandey, G.R. Bell, J.P. Rourke, A.M. Sanchez, M.D. Elkin, B.J. Hickey, N.R. Wilson, Physical vapor deposition of metal nanoparticles on chemically modified graphene: observations on metal-graphene interactions, Small 7 (22) (2011) 3202–3210.
[16] J.L. Lu, H.J. Gao, S. Shaikhutdinov, H.J. Freund, Gold supported on well-ordered ceria films: nucleation, growth and morphology in CO oxidation reaction, Catal. Lett. 114 (1) (2007) 8–16.
[17] H. Wu, D. Kong, Z. Ruan, P.-C. Hsu, S. Wang, Z. Yu, T.J. Carney, L. Hu, S. Fan, Y. Cui, A transparent electrode based on a metal nanotrough network, Nat. Nanotechnol 8 (6) (2013) 421–425.
[18] A. Miyamoto, S. Lee, N.F. Cooray, S. Lee, M. Mori, N. Matsuhisa, H. Jin, L. Yoda, T. Yokota, A. Itoh, M. Sekino, H. Kawasaki, T. Ebihara, M. Amagai, T. Someya, Inflammation-free, gas-permeable, lightweight, stretchable on-skin electronics with nanomeshes, Nat. Nanotechnol 12 (9) (2017) 907–913.
[19] K.L. Choy, Chemical vapour deposition of coatings, Prog. Mater Sci. 48 (2) (2003) 57–170.
[20] A. Grodzicki, I. Łakomska, P. Piszczek, I. Szymańska, E. Szłyk, Copper(I), silver(I) and gold(I) carboxylate complexes as precursors in chemical vapour deposition of thin metallic films, Coord. Chem. Rev. 249 (21) (2005) 2232–2258.
[21] M. Jung, G. Lee, J. Choi, Electrochemical plating of Cu-Sn alloy in non-cyanide solution to substitute for Ni undercoating layer, Electrochim. Acta 241 (2017) 229–236.
[22] S. Sinha-Ray, Y. Zhang, A.L. Yarin, Thorny Devil Nanotextured Fibers: the way to cooling rates on the order of 1 kW/cm2, Langmuir 27 (1) (2011) 215–226.
[23] O. Azzaroni, Z. Zheng, Z. Yang, W.T.S. Huck, Polyelectrolyte Brushes as efficient ultrathin platforms for site-selective copper electroless deposition, Langmuir 22 (16) (2006) 6730–6733.
[24] X. Cauchy, J.-E. Klemberg-Sapieha, D. Therriault, Synthesis of highly conductive, uniformly silver-coated carbon nanofibers by electroless deposition, ACS Appl. Mater. Interfaces 9 (34) (2017) 29010–29020.
[25] F. Muench, S. Schaefer, L. Hagelüken, L. Molina-Luna, M. Duerrschnabel, H.-J. Kleebe, J. Brötz, A. Vaskevich, I. Rubinstein, W. Ensinger, Template-free electroless plating of gold nanowires: direct surface functionalization with shape-selective nanostructures for electrochemical applications, ACS Appl. Mater. Interfaces 9 (36) (2017) 31142–31152.
[26] D. Zabetakis, W.J. Dressick, Selective electroless metallization of patterned polymeric films for lithography applications, ACS Appl. Mater. Interfaces 1 (1) (2009) 4–25.
[27] D. Alique, D. Martinez-Diaz, R. Sanz, J.A. Calles, Review of supported Pd-based membranes preparation by electroless plating for ultra-pure hydrogen production, Membranes 8 (1) (2018) 5.
[28] X, Wang, T, Xu, M.J, de Andrade, I, Rampalli, D, Cao, M, Haque, S, Roy, R.H, Baughman, H, Lu, The Interfacial Shear Strength of Carbon Nanotube Sheet Modified Carbon Fiber Composites, in: M, Silberstein, A. Amirkhizi (Eds.) Challenges in Mechanics of Time Dependent Materials, Volume 2, Springer International Publishing, Cham, 2021, pp. 25-32.
[29] L. Supriya, R.O. Claus, Solution-based assembly of conductive gold film on flexible polymer substrates, Langmuir 20 (20) (2004) 8870–8876.
[30] C.M. Gabardo, R.C. Adams-McGavin, B.C. Fung, E.J. Mahoney, Q. Fang, L. Soleymani, Rapid prototyping of all-solution-processed multi-lengthscale electrodes using polymer-induced thin film wrinkling, Sci Rep 7 (2017) 42543.
[31] J. Hu, W. Li, J. Chen, X. Zhang, X. Zhao, Novel plating solution for electroless deposition of gold film onto glass surface, Surf. Coat. Technol. 202 (13) (2008) 2922–2926.
[32] E. Malel, D. Mandler, Localized electroless deposition of gold nanoparticles using scanning electrochemical microscopy, J. Electrochemical Soc. 155 (6) (2008) D459.
[33] X. Wei, D.K. Roper, Tin sensitization for electroless plating review, J. Electrochem. Soc. 161 (5) (2014) D235–D242.
[34] R. Sard, The nucleation, growth, and structure of electroless copper deposits, J. Electrochem. Soc. 117 (7) (1970) 864.
[35] D.R. Merkel, C.M. Laursen, C.M. Yakacki, R.A. Rorrer, C.P. Frick, Characterization and mechanical testing of polydopamine-adhered electroless copper films, Surface and Coatings Technol. 331 (2017) 211–220.
[36] J.H. Ryu, P.B. Messersmith, H. Lee, Polydopamine surface chemistry: a decade of discovery, ACS Appl. Mater. Interfaces 10 (9) (2018) 7523–7540.
[37] D. Cao, Z. Fu, C. Li, Heat and compression molded electrospun poly(l-lactide) membranes: preparation and characterization, Mater. Sci. Eng., B 176 (12) (2011) 900–905.
[38] S.K. Sivaraman, S. Kumar, V. Santhanam, Monodisperse sub-10 nm gold nanoparticles by reversing the order of addition in Turkevich method–The role of chloroauric acid, J. Colloid Interface Sci. 361 (2) (2011) 543–547.
[39] V.P. Menon, C.R. Martin, Fabrication and Evaluation of Nanoelectrode Ensembles, Anal. Chem. 67 (13) (1995) 1920–1928.
[40] X. Liu, H. Xu, H. Xia, D. Wang, Rapid Seeded Growth of Monodisperse, Quasi-Spherical, Citrate-Stabilized Gold Nanoparticles via H2O2 Reduction, Langmuir 28 (38) (2012) 13720–13726.
[41] S.A. Hosseini, H.V. Tafreshi, Modeling permeability of 3-D nanofiber media in slip flow regime, Chem. Eng. Sci. 65 (6) (2010) 2249–2254.
[42] Z. Tan, Basic properties of gases, Air Pollution and Greenhouse Gases, Springer, 2014, pp. 27–58.
[43] R. Kas, R. Kortlever, H. Yılmaz, M.T.M. Koper, G. Mul, Manipulating the Hydrocarbon Selectivity of Copper Nanoparticles in CO2 electroreduction by process conditions, ChemElectroChem. 2 (3) (2015) 354–358.
[44] H. Zhong, K. Fujii, Y. Nakano, F. Jin, Effect of CO2 Bubbling into Aqueous Solutions Used for Electrochemical Reduction of CO2 for Energy Conversion and Storage, J. Phys. Chem. C 119 (1) (2015) 55–61.
[45] Y, Hori, A, Murata, R, Takahashi, Formation of hydrocarbons in the electrochemical reduction of carbon dioxide at a copper electrode in aqueous solution, J, Chem. Soc., Faraday Trans. 1 85 8 1989 2309 2326.
[46] R.G. Freeman, K.C. Grabar, K.J. Allison, R.M. Bright, J.A. Davis, A.P. Guthrie, M.B. Hommer, M.A. Jackson, P.C. Smith, D.G. Walter, M.J. Natan, Self-Assembled Metal Colloid Monolayers: an approach to SERS Substrates, Science 267 (5204) (1995) 1629–1632.
[47] J. Zeng, K. Bejtka, W. Ju, M. Castellino, A. Chiodoni, A. Sacco, M.A. Farkhondehfal, S. Hernández, D. Rentsch, C. Battaglia, C.F. Pirri, Advanced Cu-Sn foam for selectively converting CO2 to CO in aqueous solution, Appl. Catal. B 236 (2018) 475–482.
[48] J.K. Nayak, P. Parhi, R. Jha, Graphene oxide encapsulated gold nanoparticle based stable fibre optic sucrose sensor, Sens. Actuators B Chem. 221 (2015) 835–841.
[49] S. Hrapovic, Y. Liu, G. Enright, F. Bensebaa, J.H.T. Luong, New Strategy for Preparing Thin Gold Films on Modified Glass Surfaces by Electroless Deposition, Langmuir 19 (9) (2003) 3958–3965.
[50] J.-P. Sylvestre, S. Poulin, A.V. Kabashin, E. Sacher, M. Meunier, J.H. Luong, Surface chemistry of gold nanoparticles produced by laser ablation in aqueous media, J. Phys. Chem. B 108 (43) (2004) 16864–16869.
[51] Y. Liu, K. Ai, L. Lu, Polydopamine and its derivative materials: synthesis and promising applications in energy, environmental, and biomedical fields, Chem. Rev. 114 (9) (2014) 5057–5115.
[52] S. Whitaker, Flow in porous media I: A theoretical derivation of Darcy's law, Transp. Porous Media 1 (1) (1986) 3–25.
[53] E.R. Cave, J.H. Montoya, K.P. Kuhl, D.N. Abram, T. Hatsukade, C. Shi, C. Hahn, J.K. Nørskov, T.F. Jaramillo, Electrochemical CO 2 reduction on Au surfaces: mechanistic aspects regarding the formation of major and minor products, PCCP 19 (24) (2017) 15856–15863.
[54] B. De Mot, J. Hereijgers, M. Duarte, T. Breugelmans, Influence of flow and pressure distribution inside a gas diffusion electrode on the performance of a flow-by CO2 electrolyzer, Chem. Eng. J. 378 (2019) 122224.
[55] K. Junge Puring, D. Siegmund, J. Timm, F. Möllenbruck, S. Schemme, R. Marschall, U.-P. Apfel, Electrochemical CO2 Reduction: tailoring catalyst layers in gas diffusion electrodes, Adv. Sustain. Syst. 5 (1) (2021) 2000088.
[56] Z. Xing, L. Hu, D.S. Ripatti, X. Hu, X. Feng, Enhancing carbon dioxide gas-diffusion electrolysis by creating a hydrophobic catalyst microenvironment, Nat. Commun. 12 (1) (2021) 136.